

Orally administrated bismuth drug together with N-acetyl cysteine as a broad-spectrum anti-coronavirus cocktail therapy

Runming Wang ^{‡a}, Jasper Fuk-Woo Chan ^{‡b,c,d,e}, Suyu Wang ^{‡a}, Hongyan Li ^a, Jiajia Zhao ^f, Tiffany Ka-Yan Ip ^a, Joan Zhong Zuo ^f, Kwok-Yung Yuen ^{b,c,d,e}, Shuofeng Yuan ^{b,c,e*}, and Hongzhe Sun ^{a*}

^a Department of Chemistry and CAS-HKU Joint Laboratory of Metallomics on Health and Environment, The University of Hong Kong, Hong Kong SAR, P.R. China. E-mail: hsun@hku.hk

^b State Key Laboratory of Emerging Infectious Diseases, Carol Yu Centre for Infection, Department of Microbiology, Li Ka Shing Faculty of Medicine, The University of Hong Kong, Pokfulam, Hong Kong SAR, China

^c Department of Clinical Microbiology and Infection Control, The University of Hong Kong-Shenzhen Hospital, Shenzhen, Guangdong Province, China

^d Hainan Medical University-The University of Hong Kong Joint Laboratory of Tropical Infectious Diseases and Academician Workstation of Hainan Province, Hainan Medical University, Haikou, Hainan, China, and The University of Hong Kong, Pokfulam, Hong Kong SAR, China.

^e Centre for Virology, Vaccinology and Therapeutics, Hong Kong Science and Technology Park, Hong Kong SAR, China

^f School of Pharmacy, Faculty of Medicine, The Chinese University of Hong Kong, Shatin, New Territories, Hong Kong SAR, China.

* Corresponding author: H. Sun (hsun@hku.hk) and S.F. Yuan (yuansf@hku.hk).

‡These authors contribute equally to this work.

Experimental Procedures

References

Figures S1-S9

Tables S1-S3

Experimental Procedures

Chemicals. Colloidal bismuth citrate (CBS) and ranitidine bismuth citrate (RBC) were kindly provided by Livzon Pharmaceutical Group. The combination of CBS and NAC was freshly prepared before experiments by physically mixing CBS and appropriate molar equivalents of NAC, followed by adjustment of pH in the range of 5-6 with 0.05 M NaOH. Bismuth subsalicylate (BSS) and bismuth subgallate (BGS) were obtained from Alfa Aesar. [Bi(NTA)] was prepared and characterized as previously described ¹. Kanamycin sulfate and Luria-Bertani (LB) Broth Powder were purchased from Affymetrix. All other chemicals were from Sigma-Aldrich unless otherwise stated. Chemical structures in schemes were generated by ChemDraw Ultra 16.0.

Cell lines and viruses. Cell lines used in this study were chosen according to their sensitivity to replication of corresponding coronavirus. Human colon Caco-2 cells purchased from American Type Culture Collection (Manassas, VA, USA) were cultured in Dulbecco's Modified Eagle's Medium (DMEM, Gibco, Grand Island, NY, USA) supplemented with 10% of fetal Bovine Serum (FBS, Gibco, Paisley, UK), 1% of penicillin–streptomycin (Gibco BRL, Grand Island, NY, USA) and 1% of non-essential amino acids (Gibco BRL, Gibco, Grand Island, NY, USA). Monkey Vero E6 cells (ATCC, CRL-1586) were cultured in DMEM supplemented with 10% FBS, 50 U/mL penicillin and 50 µg/mL streptomycin. Human embryonic lung fibroblasts (HELFL) were developed in-house. Cells were maintained at 37 °C, in an atmosphere of 5% CO₂ and 90% relative humidity.

SARS-CoV-2 virus HKU-001a (GenBank: MT230904) and B.1.1.7 (GISAID: EPI_ISL_1273444) were clinical isolate as previously described². In brief, the nasopharyngeal aspirate specimen from a patient with laboratory-confirmed COVID-19 in Hong Kong was inoculated on Vero E6 cells (ATCC CRL-1586). The inoculated cells were monitored daily for cytopathic effects by light microscopy and the cell supernatants were collected daily for qRT-PCR to assess viral load. The virus was passaged three times before being used for the experiments. MERS-CoV (EMC/2012) was kindly provided by Ron Fouchier (Erasmus Medical Center, the Netherlands)³. Archived clinical strain of HCoV-229E was obtained from the Department of Microbiology, The University of Hong Kong⁴.

Live subject statement. All experiments were approved by, and performed in accordance with the guidelines approved by Committee on the Use of Live Animals in Teaching and Research (CULATR) of the University of Hong Kong and the Animal Ethics Committee of the Chinese University of Hong Kong. No experimentation with human subjects were involved in current study.

For mouse experiments, 6-to-8-week-old female BALB/c mice with body weight of 18-22 g, were purchased from Charles River Laboratories, Inc. All animal procedures were approved by CULATR of the University of Hong Kong (reference code: CULATR 5079-19). For rat related experiments, Sprague Dawley rats with body weight of 200-220 g, were supplied by the Laboratory Animal Services Center at the Chinese University of Hong Kong. The animal experiments were conducted under the approval of Animal Ethics Committee of the Chinese University of Hong Kong (reference code: 19/074/GRF-5-C & (19-589) in DH/SHS/8/2/1 Pt.22) All the animals were randomly caged in biosafety level housing and given access to standard pellet feed and water ad libitum before the commence of corresponding experiments.

For hamster experiments, 6-to-10-week-old male and female Syrian hamsters with body weight of 70-100 g, were obtained from the Chinese University of Hong Kong Laboratory Animal Service Centre through the HKU Centre for Comparative Medicine Research. The hamsters were kept in biosafety level 2 housing and given access to standard pellet feed and water ad libitum, as previously described^{5, 6}. All experimental protocols were approved by the CULATR of the University of Hong Kong and were performed according to the standard operating procedures of the biosafety level 3 animal facilities (reference code: CULATR 5370-20).

Antiviral assessment in a hamster model of SARS-CoV-2 infection. Each hamster was intranasally inoculated with 10^5 p.f.u. of SARS-CoV-2 (SARS-CoV-2 HKU-001a) in 100 μ L PBS under intraperitoneal ketamine (200 mg per kg body weight) and xylazine (10 mg per kg body weight) anaesthesia. From -2 day-post-infection (dpi) to 1 dpi, hamsters were orally administered once daily with water as vehicle, CBS (300 mg/kg) or BSS (300 mg/kg), NAC (370 mg/kg), CBS (300 mg/kg)+3NAC (370 mg/kg) or BSS (300 mg/kg)+3NAC (405 mg/kg),

respectively, for four consecutive days. Animals were monitored twice daily for clinical signs of disease. Eight or four animals in each group were euthanized at 2 dpi. for virological and histopathological analyses. Lung tissue samples were isolated. Viral yield in the tissue homogenates was detected by qRT-PCR methods. The cytokine and chemokine profiles of the hamster lungs were detected by the $2^{-\Delta\Delta CT}$ method using probe-based one-step qRT-PCR (Qiagen). The tissue pathology of infected animals was examined by H&E and immunofluorescence staining in accordance with an established protocol⁷

Immunofluorescence microscopy. Vero E6 cells were infected with SARS-CoV-2 (MOI=0.1) and exposed to the treatment of water as vehicle, CBS (1000 μ M), NAC (1000 μ M), and CBS (1000 μ M)+3NAC (3000 μ M), respectively, for 24 hours. Antigen expression in the infected cells was detected with an in-house rabbit antiserum against SARS-CoV-2-nucleocapsid protein (NP) of SARS-CoV-2. Cell nuclei were labelled with the 4,6-diamidino-2-phenylindole (DAPI) nucleic acid stain (Thermo Fisher Scientific). The Alexa Fluor secondary antibodies were obtained from Thermo Fisher Scientific. Mounting was performed with the Diamond Prolong AntiFade mountant from Thermo Fisher Scientific.

Nephrotoxicity test. Groups of mice (n=4 per group) were orally administered with water as vehicle, CBS (500 mg/kg) and CBS (500 mg/kg)+3NAC (580 mg/kg) 4 consecutive days, respectively. Mice were sacrificed at 1, 7, 14, 28 day post last dosing and mice serum was collected for the blood urea nitrogen test (ThermoFisher, USA) and creatinine test (Cayman Chemical, MI, USA) according to the manufacturer's instruction. Serum isolated from untreated mice were used as control.

Viral load reduction assay. Viral load reduction assay was performed for the evaluation of antiviral potency⁸. Briefly, SARS-CoV-2-infected (MOI = 0.01) Vero E6 cells were treated with different concentrations of either CBS or CBS+3NAC. Cell culture supernatants were collected at 48 hour-post-infection (hpi) for viral RNA extraction and quantitative reverse transcription-polymerase chain reaction (qRT-PCR) as previously described with modifications^{9, 10}. The primers and probe sequences were against the RNA-dependent RNA polymerase/Helicase (RdRP/Hel) gene region of SARS-CoV-2: forward primer: 5'-CGCATAACAGTCTTRCAGGCT-3'; reverse primer: 5'-GTGTGATGTTGAWATGACATGGTC-3';

specific probe: 5'-FAMTTAAGATGTGGTGCTTGCATACGTAGAC-IABkFQ-3'. The viral load reduction assay experiments were performed in triplicate and repeated twice for confirmation.

Plaque reduction assay. Plaque reduction assay was performed to estimate the half maximal effective concentration (EC_{50}) as previously described with slight modifications^{6, 11}. Briefly, VeroE6 cells were seeded at 4×10^5 cells/well in 12-well tissue culture plates on the day before the assay was performed. After 24 hour of incubation, 50 plaque-forming units (PFU) of SARS-CoV-2 were added to the cell monolayer with or without the addition of CBS, NAC or CBS+3NAC at varying concentrations. The plates were further incubated for 1 hour at 37°C in 5% CO₂ before removal of unbound viral particles by aspiration of the media and washing once with DMEM. Monolayers were then overlaid with media containing 1% low melting agarose (Cambrex Corporation, New Jersey, USA) in DMEM and appropriate concentrations of trichostatin A, inverted and incubated as above for another 72 hours. The wells were then fixed with 10% formaldehyde (BDH, Merck, Darmstadt, Germany) overnight. After removal of the agarose plugs, the monolayers were stained with 0.7% crystal violet (BDH, Merck) and the plaques were counted. The percentage of plaque inhibition relative to the control (*i.e.* without the addition of compound) wells was determined for each concentration of drug compound. EC_{50} was calculated using Sigma plot (SPSS) in an Excel add-in ED50V10. The plaque reduction assay experiments were performed in triplicate and repeated twice for confirmation.

Analyses of bismuth by inductively coupled plasma mass spectroscopy (ICP-MS). ICP-MS was used to monitor the levels of bismuth in all investigated subjects. A quadrupole-based inductively coupled plasma mass spectroscopy (ICP-MS) (Agilent 7700x, Agilent Technologies, CA), equipped with a glass concentric nebulizer was used in this study. The samples were diluted to an appropriate concentration, sprayed into aerosols using microconcentric nebulizer and introduced into the ICP directly for time-resolved ICP-MS measurements. Samples were further diluted when the measured signals exceeded the linear range of standard curve. Bismuth contents (Bi^{209}) in the investigated substance were

calculated according to the standard curve in 1% nitric acid or respective blank control solution of organ and blood. Only one isotope was monitored in each measurement.

The main parameters were listed as follows: RF power (1300 kW); spray chamber (Scott spray chamber); nebulizer (MicroMist nebulizer); lens: (Ni); nebulizer gas flow (0.8 mL/min); acquisition mode: TRA (Time Resolved Analysis); dwell time: 100 ms; reaction gas (no gas); temperature (2 °C). Bismuth standard solutions were prepared by diluting Multielement Calibration Standard (Fluka Analytical, 90243). The internal standard (10 µg L⁻¹; Agilent Technologies, 5188–6525) was used during the measurement.

Chemical stability. Simulated gastric fluid, phosphate buffered saline and sodium bicarbonate buffer were applied to mimic environment in pH 1.2, 7.4 and 9.2. The simulated gastric fluid was prepared by dissolving NaCl (0.2 g) and pepsin (0.32 g) in about 70 mL of deionized water. The pH was then adjusted to 1.2 with 10 M HCl. The volume was finally adjusted to 100 mL with deionized water. Phosphate buffered saline was made from 2.7 mM potassium chloride, 1.8 mM monopotassium phosphate, 137 mM sodium chloride and 10 mM disodium phosphate. The pH was adjusted to 7.4 with HCl. Sodium bicarbonate solution (150 mM) was prepared by dissolving NaHCO₃ into deionized water and the pH was adjusted to 9.2.

To monitor the stability of bismuth-NAC in different pH, bismuth-NAC mixtures were prepared in ratios of 1:1, 1:3 and 1:10 by adding appropriate amount of NAC into 10 mM CBS solution. Each bismuth-NAC (in a aliquot of 500 µL) was mixed with equal volume of the pH buffer and incubated for 24 hours. The mixtures were centrifuged, and each supernatant was aliquoted into separated tube as samples which were subsequently subjected to ICP-MS for the measurement of remaining bismuth content in the supernatant.

Bismuth-thiol mixtures were prepared by titration of NAC to solutions of bismuth drugs. Mixtures of Bi-NAC in a ratio of 1:3 were prepared by adding appropriate amounts of NAC into solution of CBS (10 mM) and RBC (10 mM), respectively. Mixtures of BSG and BSS with NAC were obtained by dissolving appropriate amounts of BSG and BSS powders in NAC (100 mM) with a molar ratio of 1:10, respectively. Photos were taken as a record and shown in **Fig. S4**.

Parallel artificial membrane permeability assay (PAMPA). PAMPA was used to determine bismuth permeation in the absence or presence of NAC. Donor (apical) solutions were prepared by adding CBS (2.5 mM), CBS (2.5 mM)+1NAC (2.5 mM), CBS (2.5 mM)+3NAC (7.5 mM), CBS(2.5 mM)+10NAC (25 mM), CBS(2.5 mM)+20NAC (50 mM) in PBS (pH 1.2). About 5 μ L of egg lecithin in dodecane (1 % w/v) were added onto the artificial membrane of each well in the donor plate for the activation of the membrane. Subsequently, 400 μ L of acceptor solution were added in each well of the acceptor plate (BioAssay System, US), and covered by the donor plate with an aliquot of 200 μ L of donor solution in each well. The system was incubated 16-hour at room temperature, followed by the measurement of bismuth concentrations of each investigated substance in starting solution, donor solution after incubation by ICP-MS. The assay was performed in triplicate.

***In vitro* Caco-2 permeability assay.** The *in vitro* permeability of CBS in the absence or presence of NAC was evaluated by using the Caco-2 permeability assay according to a method as described previously¹².

Briefly, Caco-2 cells with 80–90% confluence was sub-cultured by trypsinization with 0.05% trypsin–EDTA (Gibco BRL, Gibco, Grand Island, NY, USA) and plated onto six-well plates Transwell inserts (24 mm i.d., 0.4 μ m pore size, 4.67 cm², polycarbonate filter, Corning Costar Co. NY, USA) coated with collagen (collagen type I rat tail solution, ST. Louis, MO, USA) at a density of 1-2 \times 10⁵ cells per well and cultured for 21 days prior to transport experiments. Transepithelial electrical resistance (TEER) value of each well was monitored by epithelial voltammeter (EVOM2, World Precision Instruments Inc., Berlin, Germany) with STX2 electrode set according to the manufacturer's instructions to ensure the integrity of the monolayer. Cell monolayer with TEER above 600 Ω cm² was used in this study.

For transport study, CBS (150 μ M) and CBS (150 μ M)+10NAC (1.5 mM) were prepared in transport buffer [Hank's balanced salt solution (pH 7.4, HBSS, Grand Island, NY, USA) with phenol red] and loaded in the donor (apical) chamber in a 1.5 mL aliquot, respectively, followed by adding 2.5 mL transport buffer in receiver (basolateral) chamber. Aliquots of 0.1 mL samples was withdrawn from the receiver chamber at different time intervals (10, 20, 30, 40, 50, 60 min) and equal volume of blank transport buffer was supplemented in

receiver chamber immediately. The assay was performed in triplicate. Samples collected from the transport study were diluted to appropriate concentrations with 1% HNO₃ followed by ICP-MS measurement of bismuth content transported from donor side to receiver side. At the end of transport study, Caco-2 cells on the monolayer were also collected after washing with PBS for six times, and the numbers of cells were counted by hemocytometer under an optical microscope. The resulting cell pellets were acidified with 69% HNO₃, and diluted appropriately for the measurement of bismuth accumulation in cells. The apparent permeability coefficients (P_{app} , cm/s) of CBS from different treatment groups were calculated through the following equation ¹³:

$$P_{app} = \frac{dQ}{dt} \times \frac{1}{A \times C}$$

where dQ/dt ($\mu\text{mol/s}$) is cumulative concentration at time t , C (μM) is the initial concentration of test drugs in the donor chamber and A (cm^2) is the surface area of the monolayer.

Ex vivo everted gut sac model. *Ex vivo* everted gut sac model was performed according to a modified method ^{14, 15}. For the preparation of everted gut sac, small intestines were rapidly isolated from rats right after their sacrificing followed by being washed several times with 0.9% saline. Duodenum was segmented of the intestine (~4 cm) in oxygenated medium [Krebs–Henseleit solution (pH 7.4, 1.25 mM NaHCO₃, pH 7.4, 5.9 mM NaCl, 23.5 μM KCl, 60 μM MgSO₄, 62.5 μM CaCl₂, 60 μM KH₂PO₄, 550 μM glucose)], gently everted, washed, slid onto a glass rod and fastened with braided silk. Duodenum was clamped at one end and filled with an aliquot of 1 mL fresh oxygenated medium, and subsequently sealed with a second clamp, resulting an everted gut sac with approximately 3 cm in length using braided silk sutures.

The everted gut sacs (n=3 per group) were dialyzed in oxygenated medium supplemented with CBS (200 μM), CBS (200 μM)+1NAC (200 μM), CBS (200 μM)+3NAC (600 μM), CBS (200 μM)+10NAC (2 mM), respectively, at 37°C. Aliquots of 50 μL samples were withdrawn from the gut sacs at different time intervals (15, 30, 45, 60 min) and equal volume of oxygenated medium was supplemented in gut sacs immediately. The length and width of each intestinal

segment was measured after the final sample was taken. Bismuth content transported into the gut sacs was measured by ICP-MS as mentioned above.

***In vivo* pharmacokinetics studies.** To estimation the impact of NAC on blood bismuth content, groups of Balb/c mice (n=3 per group) were orally administered with CBS (150 mg/kg), CBS (150 mg/kg)+3NAC (180 mg/kg), CBS (150 mg/kg)+10NAC (610 mg/kg), CBS (150 mg/kg)+20NAC (1220 mg/kg), respectively. Mice were sacrificed at 0.5-hour and 1-hour post-dosing and ~600 μ L of blood per mouse were collected in heparinized centrifuge tubes. Blood was acidified with HNO₃ and subjected to ICP-MS for bismuth content measurement. Blood from untreated mice was collected and used as control to eliminate matrix effects. For the measurement of bismuth accumulation in mouse lung, groups of Balb/c mice (n=3 per group) were orally administered with CBS (150 mg/kg)+10NAC (610 mg/kg) for 1 day, consecutive 2 days, consecutive 3 days. The lung tissues were dissected after cardiac perfusion with 0.9% saline, and acidified with 69%HNO₃ for the measurement of bismuth content by using ICP-MS.

For the measurement of detailed pharmacokinetics profiles of the optimal NAC combination with CBS identified from the above mice study, rats received a minor surgery of cannulation one day prior to experiment, with a polythene tube (i.d.0.4 mm \times o.d. 0.8 mm, Harvard Apparatus, USA) in the left jugular vein, followed by an overnight recovery and fasting. Two group of rats (n=5 per group) were orally administrated with 1-mL aliquot of CBS (150 mg/kg) or CBS (150 mg/kg)+10NAC (610 mg/kg). About 200 μ L of rat blood were collected *via* the jugular vein cannula into a heparinized centrifuge tube at 0.17, 0.33, 0.5, 1, 2, 4, 6, 8, 12, 24-hour post drug administration for respective group. Rats were allowed for free access to food 12h after drug administrations. All the rats were sacrificed 24-hour post dosing followed by cardiac perfusion with 200-mL saline to collect major organs including spleen, liver, lung, kidney and brain for further analyses. For the digestion of tissues, a modified protocol from US EPA 3050B (USEPA, 1996) was used. Briefly, approximate 0.2~0.3 g of the respective rat organ samples was placed in 15 mL polypropylene tubes and digested with 1 mL of 69% HNO₃ at 65 $^{\circ}$ C for 16 h, while 100 μ L of rat blood was digested with equal volume of 69% HNO₃ at 65 $^{\circ}$ C for 16 h. After being cooled down to room temperature, the samples

were diluted to 1% nitric acid to the final volume of 3 mL for further use. To eliminate matrix effect, blood and organs were also collected from untreated rats and digested under identical condition serving as blank control. Standard solutions were prepared by diluting multielement calibration standard of bismuth in the respective blank control of organ and blood, respectively. The bismuth content in each organ or blood sample was then measured by ICP-MS and calculated according to the standard curve in respective blank control. Pharmacokinetic parameters including the peak concentration (C_{max}), the area under the concentration-time curve (AUC), the time reaching C_{max} (T_{max}) were determined through noncompartmental analysis with Phoenix WinNonlin version 6.4 (Pharsight Corporation, Mountain View, CA, USA).

Time-of-drug-addition assay. A time-of-drug-addition assay was performed to investigate which steps of the SARS-CoV-2 replicative cycle was affected by CBS+3NAC. In brief, Vero E6 cells were seeded in 96-well plates (4×10^4 cells per well). The cells were infected by SARS-CoV-2 HKU-001a at an MOI of 1.5 and then incubated for additional 1 hour. The viral inoculum was then removed, and the cells were washed twice with PBS. At 1 hour after inoculation (that is, after entry), CBS+3NAC at a concentration of 1000 μ M was added to the infected cells at time points indicated, followed by incubation at 37 °C in 5% CO₂ until 10 hours after inoculation (that is, one complete virus life cycle). Cells were fixed at 10 hours after inoculation for the quantification of the percentage of infected cells using an immunofluorescence assay targeting SARS-CoV-2 NP.

Protein purification. The gene cloning and protein purification were performed according to previously described method^{16, 17}. Genes encoding SARS-CoV-2 papain-like protease (PL^{Pro}) (ORF1ab polyprotein residues 1564-1882), main protease (M^{Pro}) (ORF1ab polyprotein residues 3264-3569) were cloned into the expression vector pETH, respectively, and Genes encoding SARS-CoV-2 helicase (Hel) (ORF1ab polyprotein residues 16237-18039) was cloned into the expression vector pET28-a(+). The recombinant proteins were overexpressed in *E. coli* BL21(DE3) and purified using the Ni²⁺-loaded HiTrap Chelating System (GE Healthcare) according to the manufacturer's instructions. The product was further purified by gel filtration using a HiLoad 16/600 Superdex 200 prep grade column (GE Life Sciences). The

purity of each protein was assessed by 12% sodium dodecyl sulfate-polyacrylamide gels (SDS-PAGE). Apo-SARS-CoV-2 PL^{pro} (20 μ M) was prepared by dialysis in Zn²⁺ chelating buffer (20 mM Tris-HCl, pH 5.0, 150 mM NaCl, 2 mM EDTA, 2 mM TCEP, 20% glycerol) and removal of excess EDTA by ultrafiltration (Amicon). The concentration of each protein was determined by using the Bicinchoninic Acid Protein Assay Kit (Sigma-Aldrich).

Enzyme activity assay. For double-strand (ds)-unwinding inhibition assay, a FRET-based assay was performed using a previously described method, with modifications. DNA oligomers were synthesized and purified by high-performance liquid chromatography: FL-Cy3 oligo (5'-TTTTTTTTTTTTTTTTTTTTTCGAGCACCGCTGCGGCTGCACC(Cy3)-3'), RL-BHQ oligo (5'-(BHQ2)GGTGCAGCCGCAGCGGTGCTCG-3') and RL oligo (5'-GGTGCAGCCGCAGCGGTGCTCG-3') (Metabion)¹⁷. Briefly, SARS-CoV-2 Hel (10 nM) was incubated with varying concentrations of CBS and CBS+3NAC in reaction buffer (20 mM Tris-HCl buffer, pH 7.4, 10 mM NaCl, 0.1 mg/mL bovine serum albumin (BSA), 5 mM MgCl₂, 0.5 mM tris(2-carboxyethyl)phosphine (TCEP), 5% glycerol) in a 96-well black polystyrene microplate (Corning) at room temperature, then 0.5 μ L of 100 mM ATP and 1.5 μ L of oligo mixture were added to achieve final concentrations of FL-Cy3:RL-BHQ oligo and RL oligo of 5 nM and 10 nM, respectively. Fluorescence (λ_{ex} = 550 nm, λ_{em} = 620 nm) was detected to determine DNA-duplex unwinding. The relative dsDNA unwinding activity was the ratio between the activity of the samples in the presence of bismuth drug and the activity of the control, and was therefore expressed as a percentage. The assay was performed in triplicate.

For ATPase activity inhibition assays, a colorimetric assay was performed by measuring the release of phosphate using on a previously described method ¹⁷ with an ATPase assay kit (ab234055, Abcam). Typically, SARS-CoV-2 Hel (2 nM) was incubated with varying concentrations of CBS and CBS+3NAC in reaction buffer (20 mM Tris-HCl, pH 6.8, 10 mM NaCl, 5 mM MgCl₂, 0.5 mM TCEP, 5% glycerol) for 30 min at room temperature, followed by the addition of ATP (2 mM) and poly(U) (0.4 mg/mL) to initiate the reaction. To a 50 μ L reaction system added 15 μ L of the reaction developer and the colour was developed for 15 min. Absorbance was measured at 650 nm to determine ATPase activity. The relative

ATPase activity was determined as the ratio between the activity of the samples in the presence of bismuth drug and the activity of the control, and was therefore expressed as a percentage. The assay was performed in triplicate.

For PL^{pro} activity inhibition assay, a FRET-based assay was performed based on a previously described method with a peptide substrate Arg-Leu-Arg-Gly-Gly↓-AMC (RLRGG↓-AMC, Bachem Bioscience)¹⁸. SARS-CoV-2 PL^{pro} (50 nM) was incubated with CBS and CBS+3NAC at varying concentrations, respectively, for 90 min in reaction buffer (50 mM HEPES, pH 7.4, 10 mM NaCl, 0.1 mg/mL BSA, 5% glycerol, 0.5 mM TCEP) at room temperature, followed by the addition of RLRGG↓-AMC (2 μM) to initiate the reaction. After another 30 min incubation, fluorescence ($\lambda_{ex} = 335$ nm, $\lambda_{em} = 460$ nm) was measured to determine PL^{pro} activity. The relative PL^{pro} activity was determined as the ratio between the activity of the samples in the presence of bismuth drug and the activity of the control sample, and was therefore expressed as a percentage. The assay was performed in triplicate.

For M^{pro} activity inhibition assay, a FRET-based assay was performed based on a previously described method with a peptide substrate Dabcyl-KTSAVLQ↓SGFRKM-E (Edans)-NH₂ (GL Biochem)^{16, 19}. SARS-CoV-2 M^{pro} (0.5 μM) was incubated with CBS and CBS+3NAC at varying concentrations, respectively, for 30 min in reaction buffer (20 mM Tris-HCl, pH 7.4, 20 mM NaCl, 0.1 mg/mL BSA, 5% glycerol, 0.5 mM TCEP) at room temperature, followed by the addition of Dabcyl-KTSAVLQ↓SGFRKM-E (20 μM) to initiate the reaction. After another 30 min incubation, fluorescence ($\lambda_{ex} = 335$ nm, $\lambda_{em} = 460$ nm) was measured to determine M^{pro} activity. The relative M^{pro} activity was determined as the ratio between the activity of the samples in the presence of bismuth drug and the activity of the control, and was therefore expressed as a percentage. The assay was performed in triplicate.

For ACE2 activity inhibition, a modified assay was performed according to the manufactory's instruction (ab273373, Abcam) with a synthetic MCA based peptide substrate to release a free fluorophore. Recombinant ACE2 (0.1 μM) was incubated with CBS, NAC and CBS+3NAC at varying concentrations, respectively, for 30 min in ACE2 assay buffer at room temperature. The substrates (2 μM) was added to the protein solutions. After another 1-hour incubation, fluorescence ($\lambda_{ex} = 320$ nm, $\lambda_{em} = 420$ nm) was measured to determine

ACE2 activity. The relative ACE2 activity was the ratio between the activity of the samples in the presence of drugs and the activity of the control, and is therefore expressed as a percentage. The assay was performed in triplicate.

Michaelis–Menten kinetics. For PL^{pro} assay, reaction mix was prepared by incubating SARS-CoV-2 PL^{pro} (20 nM) with CBS+3NAC (0, 0.1, 0.5, 1 and 2 mM) in the reaction buffer (50 mM HEPES, pH 7.4, 10 mM NaCl, 0.1 mg/mL BSA, 5% glycerol, 0.5 mM TCEP) in a total volume of 100 μ L at room temperature for 4 hours. To each aliquot of reaction mix, substrate RLRGG↓-AMC was added to achieve final concentrations of 0.5, 1, 2, 5, 10, 20 μ M. The control experiment was performed in the absence of inhibitors under the same conditions.

For M^{pro} assay, reaction mix was prepared by incubating SARS-CoV-2 PL^{pro} (0.5 μ M) with CBS+3NAC (0, 2, 10, 20 μ M) in the reaction buffer (20 mM Tris-HCl, pH 7.4, 10 mM NaCl, 0.1 mg/mL BSA, 5% glycerol, 0.5 mM TCEP) in a total volume of 100 μ L at room temperature for 4 hours. To each aliquot of reaction mix, substrate Dabcyl-KTSAVLQ↓SGFRKM-E was added to achieve final concentrations of 10, 25, 50, 75, 100, 150, 200 μ M. The control experiment was performed in the absence of inhibitors under the same conditions. The values of V_{max} , K_m and K_i for both uninhibited and inhibited reactions were obtained by fitting the data into the double reciprocal Lineweaver–Burk plots.

Reaction kinetics of Bi³⁺ with proteins. Kinetics of reaction of Bi³⁺ with PL^{pro} and M^{pro} were performed by UV-vis spectrophotometry. Briefly, protein (SARS-CoV-2 PL^{pro}: 20 μ M, SARS-CoV-2 M^{pro}: 30 μ M) were firstly prepared in an aliquot of 50 μ L of reaction buffer (20 mM Tris-HCl, pH 7.4, 10 mM NaCl, 5% glycerol, 0.2 mM TCEP) in a 96-well UV-transparent microplates (Corning®) and then incubated with equal volume of reaction buffer supplemented with 20 mol eq. CBS. The absorbance was recorded at a fixed wavelength of 340 nm for 20 hours at room temperature. The equilibrium situation was monitored in a kinetics mode using a SpectraMax iD3 multimode microplate reader. The kinetic data were analysed by a nonlinear square fitting based on a one-phase exponential function using Prism 8.0 (GraphPad Software Inc.) software.

UV–vis spectroscopy. UV–vis spectroscopic titration was carried out on a Varian Cary 50 spectrophotometer at a rate of 360 nm min⁻¹ using a 1-cm quartz cuvette at 25 °C.

For the stoichiometry of Bi^{3+} binding to NAC, appropriate amounts of 10 mM CBS stock solution were added to a 1-mL aliquot of 500 μM NAC in titration buffer [20mM Tris-HCl, pH 5.2] to generate varying molar ratios of Bi^{3+} to NAC. The samples were left 3 min between each detection. The absorbance at 350 nm, which showed the typical Bi-S ligand-to-metal-charge-transfer band, was recorded. The stoichiometry of Bi-NAC was estimated from the titration curve.

For the stoichiometry of Bi-apo-SARS-CoV-2 PL^{pro} and Bi- SARS-CoV-2 M^{pro}, aliquots of 2 mM Bi^{3+} [as Bi(NTA)] stock solution were stepwise titrated into protein solution (final concentration of apo-SARS-CoV-2 PL^{pro}: 10 μM or SARS-CoV-2 M^{pro} : 20 μM) in titration buffer (20 mM Tris-HCl, pH 7.4, 10 mM NaCl, 1 mM TCEP) and UV-vis spectra were recorded in a range of 250–600 nm at appropriate time intervals between each addition. The binding of Bi^{3+} to the tested protein was monitored by the increase in absorption at ~ 340 nm. The UV curve was fitted with the Ryan–Weber nonlinear equation to estimate dissociation constant (K_d).

Electrospray Ionisation Mass Spectrometry (ESI-MS). Appropriate amount of bismuth nitrate was added to the water containing 3 mol eq. NAC under vigorous stirring at 25 °C for 30 min. The pH of resulting solution was adjust to ~ 1 with NaHCO_3 and then subject to Electrospray Ionization Mass Spectrometer (ESI-MS) acquisition in methanol, which was carried out on a LCQ spectrometer (Finnigan).

Zinc release assays. The release of Zn^{2+} from SARS-CoV-2 PL^{pro} upon bismuth drug exposure was perform by a previously described method with zinc-specific fluorophore FluoZinTM-3 (Invitrogen/Life Technologies)²⁰. Briefly, SARS-CoV-2 PL^{pro} (20 μM) was incubated with 0, 1, 2, 5, 20 mol eq. Bi^{3+} (as CBS), for 180 min at room temperature, followed by the addition of FluoZinTM-3 (1 μM) in a total reaction volume of 100 μL (50 mM Tris-HCl, pH 7.4, 0.1 mM TCEP, 10 mM NaCl, 5% glycerol) at room temperature. Fluorescence ($\lambda_{\text{ex}} = 494$ nm, $\lambda_{\text{em}} = 530$ nm) was detected after appropriate dilutions, and the signals were converted into Zn^{2+} concentrations using standard curves prepared from ZnSO_4 under identical condition. The signals of CBS at corresponding concentrations after mixing with FluoZinTM-3 were recorded for background subtraction. The assay was performed in

triplicate and the results were plotted as the $[\text{Released Zn}^{2+}]/[\text{SARS-CoV-2 PL}^{\text{pro}}]$ verse $[\text{Bi}^{3+}]/[\text{SARS-CoV-2 PL}^{\text{pro}}]$.

Ellman's assay. Amount of free cysteine was assayed spectrophotometrically with DTNB [5,5'-dithiobis-(2-nitrobenzoic acid)] according to a previously described method²¹. Briefly, SARS-CoV-2 M^{pro} (15 μM) was incubated with 0, 2, 5, 20 mol eq. Bi^{3+} (as CBS) in an aliquot of 50 μL reaction buffer (20 mM Tris-HCl, pH 7.4, 10 mM NaCl, 5% glycerol) in a 96-well microplate for 60 min at room temperature. Equal volume of DTNB (2 mM) was added to the reaction mix in a total reaction volume of 100 μL . After 90 min- incubation, absorption of 412 nm which indicated the release of 5-thiobenzoate anion, was detected and converted into thiol concentrations using standard curves prepared with reduced glutathione (GSH) under identical condition. The assay was performed in triplicate and the results were plotted as the $[\text{Free cysteine}]/[\text{SARS-CoV-2 M}^{\text{pro}}]$ verse $[\text{Bi}^{3+}]/[\text{SARS-CoV-2 M}^{\text{pro}}]$.

Statistical analysis. All statistical analyses were performed on three independent experiments, or more if otherwise stated, using Prism 8.0 (GraphPad Software Inc.) software.

Reference

1. S. P. Summers, K. A. Abboud, S. R. Farrah and G. J. Palenik, *Inorg. Chem.*, 1994, **33**, 88-92.
2. H. Shuai, J. F. Chan, T. T. Yuen, C. Yoon, J. C. Hu, L. Wen, B. Hu, D. Yang, Y. Wang, Y. Hou, X. Huang, Y. Chai, C. C. Chan, V. K. Poon, L. Lu, R. Q. Zhang, W. M. Chan, J. D. Ip, A. W. Chu, Y. F. Hu, J. P. Cai, K. H. Chan, J. Zhou, S. Sridhar, B. Z. Zhang, S. Yuan, A. J. Zhang, J. D. Huang, K. K. To, K. Y. Yuen and H. Chu, *EBioMedicine*, 2021, **73**, 103643.
3. S. van Boheemen, M. de Graaf, C. Lauber, T. M. Bestebroer, V. S. Raj, A. M. Zaki, A. D. Osterhaus, B. L. Haagmans, A. E. Gorbalenya, E. J. Snijder and R. A. Fouchier, *mBio*, 2012, **3**, e00473-12.
4. S. K. P. Lau, D. C. Lung, E. Y. M. Wong, K. L. Aw-Yong, A. C. P. Wong, H. K. H. Luk, K. S. M. Li, J. Fung, T. T. Y. Chan, J. Y. M. Tang, L. Zhu, C. C. Y. Yip, S. C. Y. Wong, R. A. Lee, O. T. Y. Tsang, K. Y. Yuen and P. C. Y. Woo, *mSphere*, 2021, **6**, e00819-20.
5. J. F. Chan, S. Yuan, A. J. Zhang, V. K. Poon, C. C. Chan, A. C. Lee, Z. Fan, C. Li, R. Liang, J. Cao, K. Tang, C. Luo, V. C. Cheng, J. P. Cai, H. Chu, K. H. Chan, K. K. To, S. Sridhar and K. Y. Yuen, *Clin. Infect. Dis.*, 2020, **71**, 2139-2149.
6. J. F.-W. Chan, A. J. Zhang, S. Yuan, V. K.-M. Poon, C. C.-S. Chan, A. C.-Y. Lee, W.-M. Chan, Z. Fan, H.-W. Tsoi, L. Wen, R. Liang, J. Cao, Y. Chen, K. Tang, C. Luo, J.-P. Cai, K.-H. Kok, H. Chu, K.-H. Chan, S. Sridhar, Z. Chen, H. Chen, K. K.-W. To and K.-Y. Yuen, *Clin. Infect. Dis.*, 2020, **71**, 2428-2446.
7. S. Yuan, H. Chu, J. F. Chan, Z. W. Ye, L. Wen, B. Yan, P. M. Lai, K. M. Tee, J. Huang, D. Chen, C. Li, X. Zhao, D. Yang, M. C. Chiu, C. Yip, V. K. Poon, C. C. Chan, K. H. Sze, J. Zhou, I. H. Chan, K. H. Kok, K. K. To, R. Y. Kao, J. Y. Lau, D. Y. Jin, S. Perlman and K. Y. Yuen, *Nat. Commun.*, 2019, **10**, 120.
8. S. Yuan, X. Yin, X. Meng, J. F.-W. Chan, Z.-W. Ye, L. Riva, L. Pache, C. C.-Y. Chan, P.-M. Lai, C. C.-S. Chan, V. K.-M. Poon, A. C.-Y. Lee, N. Matsunaga, Y. Pu, C.-K. Yuen, J. Cao, R. Liang, K. Tang, L. Sheng, Y. Du, W. Xu, C.-Y. Lau, K.-Y. Sit, W.-K. Au, R. Wang, Y.-Y. Zhang, Y.-D. Tang, T. M. Clausen, J. Pihl, J. Oh, K.-H. Sze, A. J. Zhang, H. Chu, K.-H. Kok, D. Wang, X.-H. Cai, J. D. Esko, I. F.-N. Hung, R. A. Li, H. Chen, H. Sun, D.-Y. Jin, R. Sun, S. K. Chanda and K.-Y. Yuen, *Nature*, 2021, DOI: 10.1038/s41586-021-03431-4.
9. S. Yuan, C. C.-Y. Chan, K. K.-H. Chik, J. O.-L. Tsang, R. Liang, J. Cao, K. Tang, J.-P. Cai, Z.-W. Ye, F. Yin, K. K.-W. To, H. Chu, D.-Y. Jin, I. F.-N. Hung, K.-Y. Yuen and J. F.-W. Chan, *Viruses*, 2020, **12**, 628.
10. S. Yuan, J. F. W. Chan, K. K. H. Chik, C. C. Y. Chan, J. O. L. Tsang, R. Liang, J. Cao, K. Tang, L. L. Chen, K. Wen, J. P. Cai, Z. W. Ye, G. Lu, H. Chu, D. Y. Jin and K. Y. Yuen, *Pharmacol Res*, 2020, **159**, 104960.
11. H. Chu, J. F.-W. Chan, Y. Wang, T. T.-T. Yuen, Y. Chai, H. Shuai, D. Yang, B. Hu, X. Huang, X. Zhang, Y. Hou, J.-P. Cai, A. J. Zhang, J. Zhou, S. Yuan, K. K.-W. To, I. F.-N. Hung, T. T. Cheung, A. T.-L. Ng, I. Hau-Yee Chan, I. Y.-H. Wong, S. Y.-K. Law, D. C.-C. Foo, W.-K. Leung and K.-Y. Yuen, *Cell. Mol. Gastroenterol. Hepatol.*, 2021, **11**, 771-781.
12. T. Ren, Q. Wang, C. Li, M. Yang and Z. Zuo, *Xenobiotica*, 2018, **48**, 1249-1257.
13. I. Hubatsch, E. G. E. Ragnarsson and P. Artursson, *Nat. Protoc.*, 2007, **2**, 2111-2119.

14. L. Barthe, J. F. Woodley, S. Kenworthy and G. Houin, *Eur. J. Drug Metab. Pharmacokinet.*, 1998, **23**, 313-323.
15. S. W. Mateer, J. Cardona, E. Marks, B. J. Goggin, S. Hua and S. Keely, *J. Vis. Exp.*, 2016, DOI: 10.3791/53250, e53250-e53250.
16. L. Wen, K. Tang, K. K.-H. Chik, C. C.-Y. Chan, J. O.-L. Tsang, R. Liang, J. Cao, Y. Huang, C. Luo, J.-P. Cai, Z.-W. Ye, F. Yin, H. Chu, D.-Y. Jin, K.-Y. Yuen, S. Yuan and J. F.-W. Chan, *Int. J. Biol. Sci.*, 2021, **17**, 1555-1564.
17. S. F. Yuan, R. M. Wang, J. F. W. Chan, A. J. X. Zhang, T. F. Cheng, K. K. H. Chik, Z. W. Ye, S. Y. Wang, A. C. Y. Lee, L. J. Jin, H. Y. Li, D. Y. Jin, K. Y. Yuen and H. Z. Sun, *Nat. Microbiol.*, 2020, **5**, 1439–1448
18. K. Ratia, S. Pegan, J. Takayama, K. Sleeman, M. Coughlin, S. Baliji, R. Chaudhuri, W. Fu, B. S. Prabhakar, M. E. Johnson, S. C. Baker, A. K. Ghosh and A. D. Mesecar, *Proc. Natl. Acad. Sci. U.S.A.*, 2008, **105**, 16119.
19. L. Zhang, D. Lin, X. Sun, U. Curth, C. Drosten, L. Sauerhering, S. Becker, K. Rox and R. Hilgenfeld, *Science*, 2020, **368**, 409.
20. K. Sargsyan, C.-C. Lin, T. Chen, C. Grauffel, Y.-P. Chen, W.-Z. Yang, H. S. Yuan and C. Lim, *Chem. Sci.*, 2020, **11**, 9904-9909.
21. H. Wang, M. Wang, X. Yang, X. Xu, Q. Hao, A. Yan, M. Hu, R. Lobinski, H. Li and H. Sun, *Chem. Sci.*, 2019, **10**, 7193-7199.

Supplementary Figures

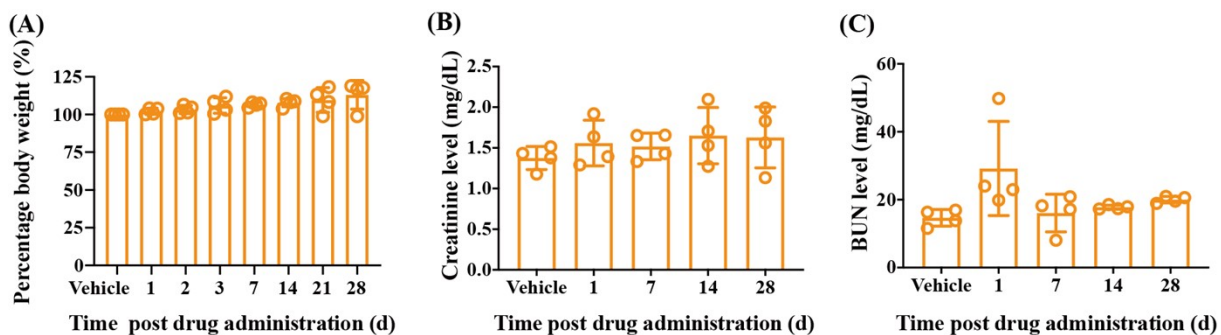


Fig. S1. Negligible or reversible neurotoxicity after CBS+3NAC administration. (A-C) Oral administration of CBS+3NAC exhibits reversible pathological change in mice kidney, as revealed by (A) Body weight changes verse time (B) BUN level versus time (n= 4) (C) creatinine level verse time (n=4). Data are shown as mean \pm SD. No difference in statistical significance was found among groups using an unpaired two-tailed Student's t-test.

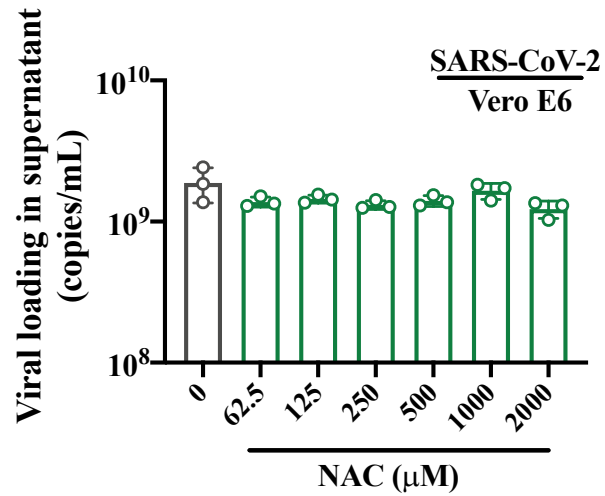


Fig. S2. Virus copies in the Vero E6 cell culture supernatant after NAC treatment (n= 3). Data are shown as mean \pm SD. No difference in statistical significance was found among groups using an unpaired two-tailed Student's t-test.

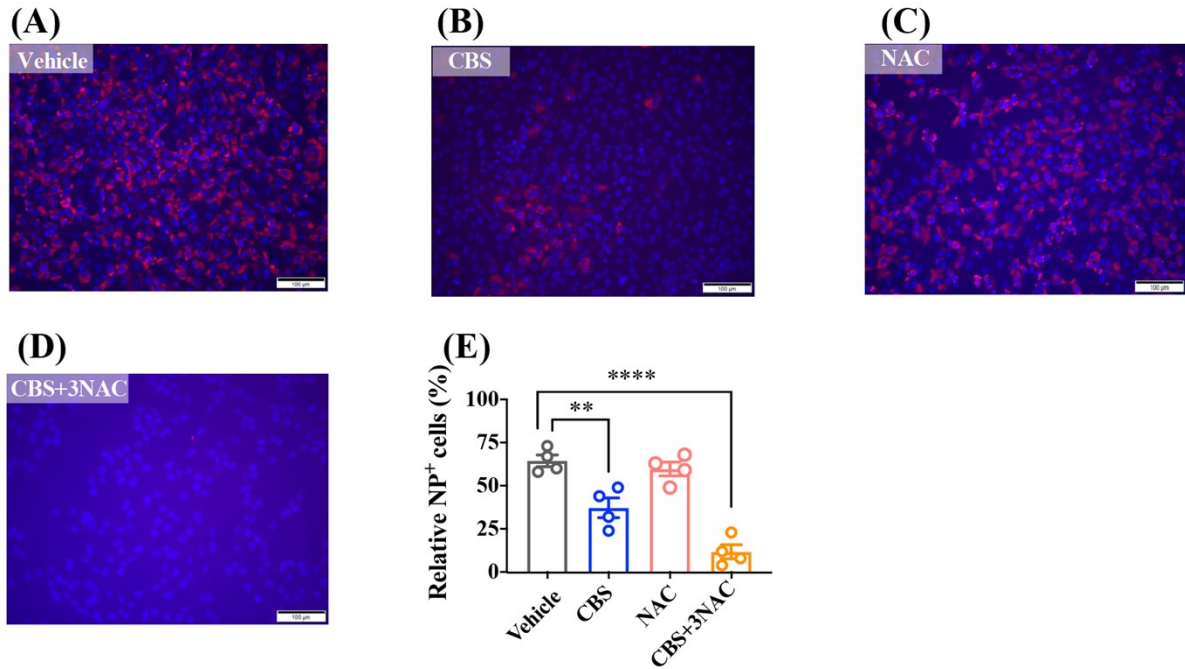


Fig. S3. Immunofluorescence assay showed antiviral potency of CBS+3NAC in cell infection model of SARS-CoV-2. (A-D) Representative immunofluorescence staining images showing the anti-SARS-CoV-2 activity of (A) vehicle, (B) CBS, (C) NAC and (D) CBS+3NAC. The nucleocapsid protein of SARS-CoV-2 (SARS-CoV-2-NP) antigens and cell nuclei (DAPI) were stained in red and blue, respectively. Scale bars: 100 μ m. (E) Quantification of NP -positive cells from randomly selected 800 \times 800-pixel fields (n= 4) over two independent experiments (one-way analysis of variance, ANOVA). ****P < 0.0001, **P < 0.01. Data are shown as mean \pm SD.

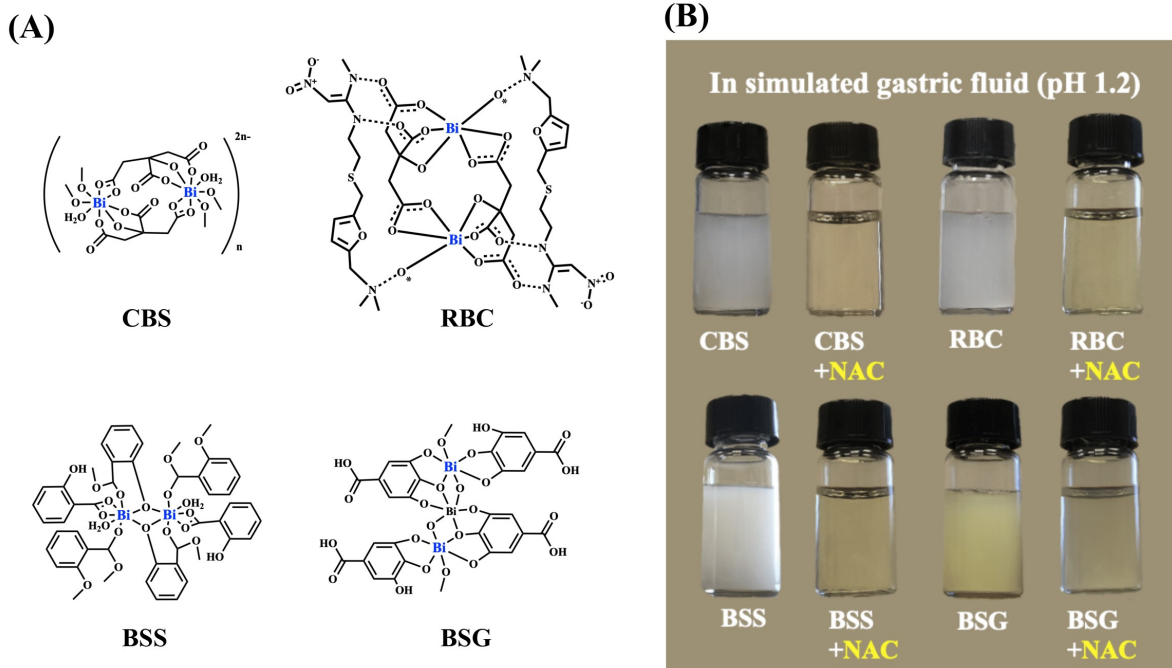


Fig. S4. (A) Structure of the basic unit of bismuth drugs. (B) Images showing that the precipitation of bismuth drugs in simulated gastric fluid (pH 1.2) was prevented in the presence of appropriate amounts of thiol-containing drugs. Abbreviation, CBS: colloidal bismuth subcitrate, NAC: N-acetylcysteine, RBC: ranitidine bismuth citrate, BSS: bismuth subsalicylate, BSG: bismuth subgallate.

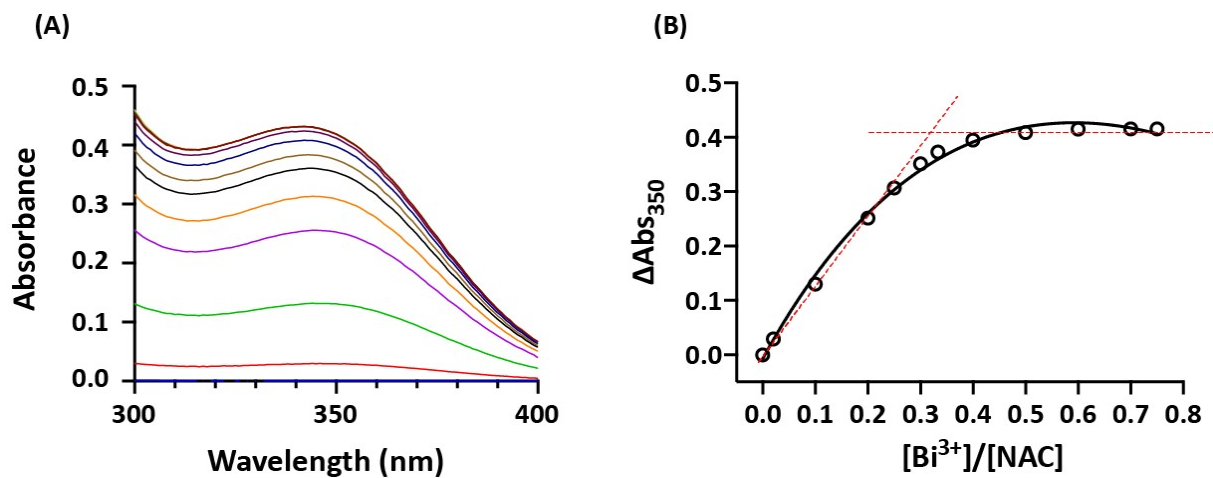


Fig. S5. (A) UV-Vis spectral profile of NAC in the absence and presence of increasing amounts of Bi^{3+} . (B) Stoichiometry of Bi^{3+} binding to NAC. UV titration curve (350 nm) for addition of CBS to CBS in titration buffer [20 mM Tris-HCl, pH 5.2, 10 mM NaCl]. The stoichiometry of Bi^{3+} to NAC was determined to be 1:3.05 from the overall absorbance changes at 350 nm, indicative of the formation of $[\text{Bi}(\text{NAC})_3]$ complex..

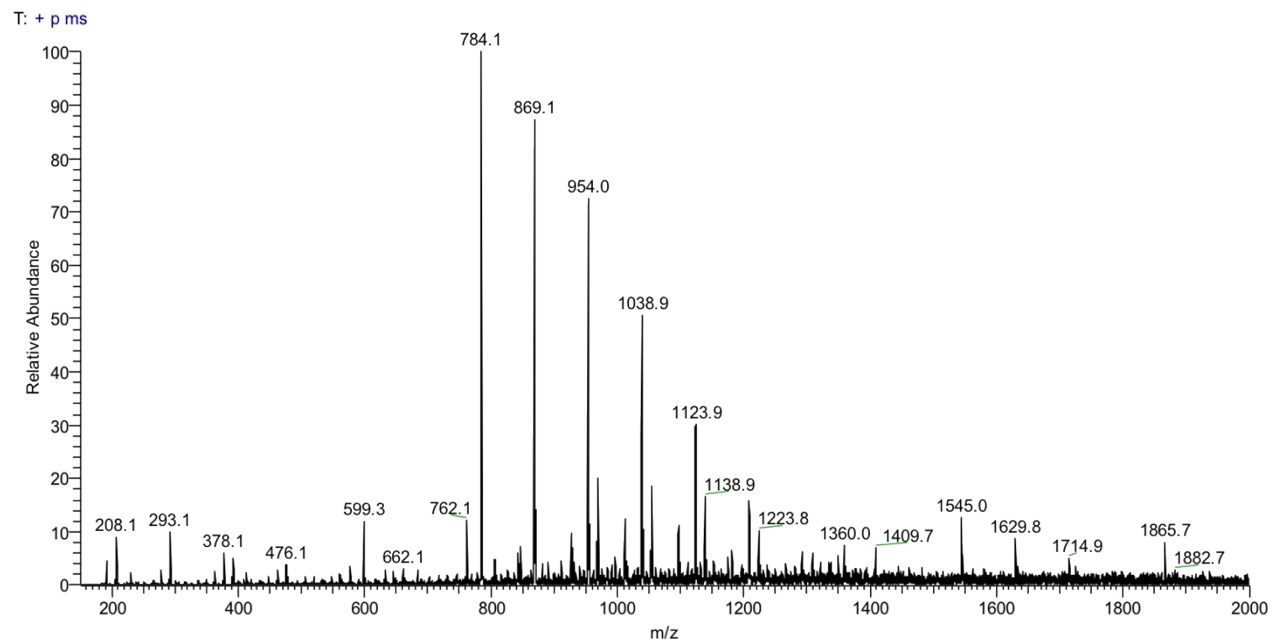


Fig. S6. A representative ESI-MS of a solution containing Bi^{3+} and NAC in a reaction stoichiometry of 1:3. ESI-MS m/z +ve: 784.1 ($[\text{Bi}(\text{NAC})_3 + \text{NaNO}_3 + \text{H}]^+$, calculated: 784.06, 100%), 869.03 ($[\text{Bi}(\text{NAC})_3 + 2(\text{NaNO}_3) + \text{H}]^+$, calculated: 869.03, 87%), 954.0 ($[\text{Bi}(\text{NAC})_3 + 3(\text{NaNO}_3) + \text{H}]^+$, calculated: 954.00, 71%), 1038.9 ($[\text{Bi}(\text{NAC})_3 + 4(\text{NaNO}_3) + \text{H}]^+$, calculated: 1038.98, 50%), 1123.9 ($[\text{Bi}(\text{NAC})_3 + 5(\text{NaNO}_3) + \text{H}]^+$, calculated: 1123.96, 30%).

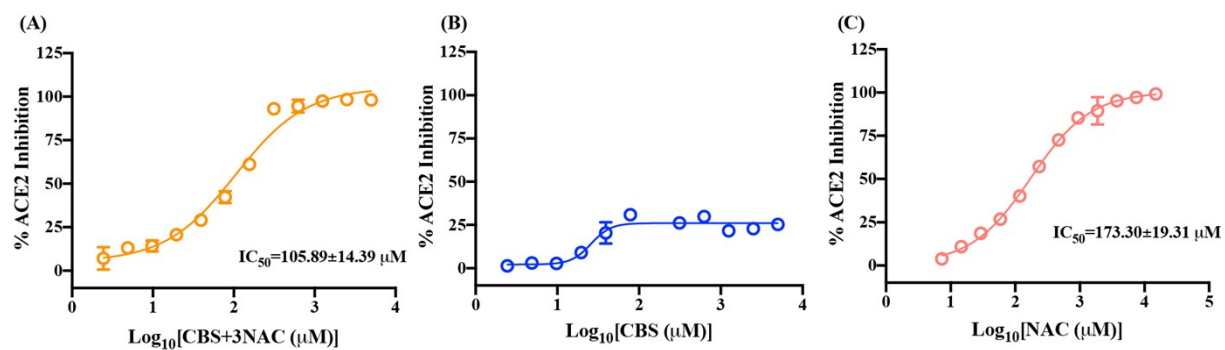


Fig. S7. Inhibition of (a) CBS+3NAC, (b) CBS and (c) NAC on ACE2 activity (n= 3). Data are shown as mean \pm SD.

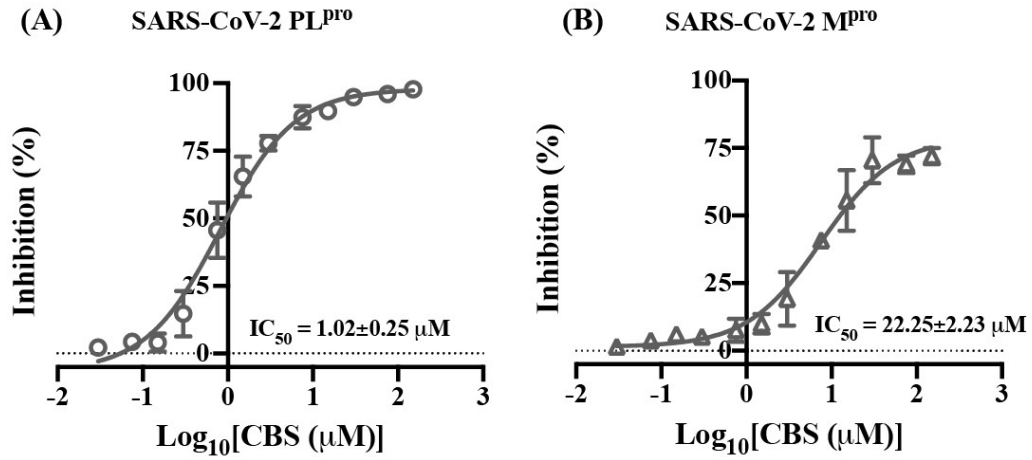


Fig. S8. Inhibition of CBS on (A) SARS-CoV-2 PL^{pro} activity (B) SARS-CoV-2 M^{pro} activity (n=3). Data are shown as mean ± SD.

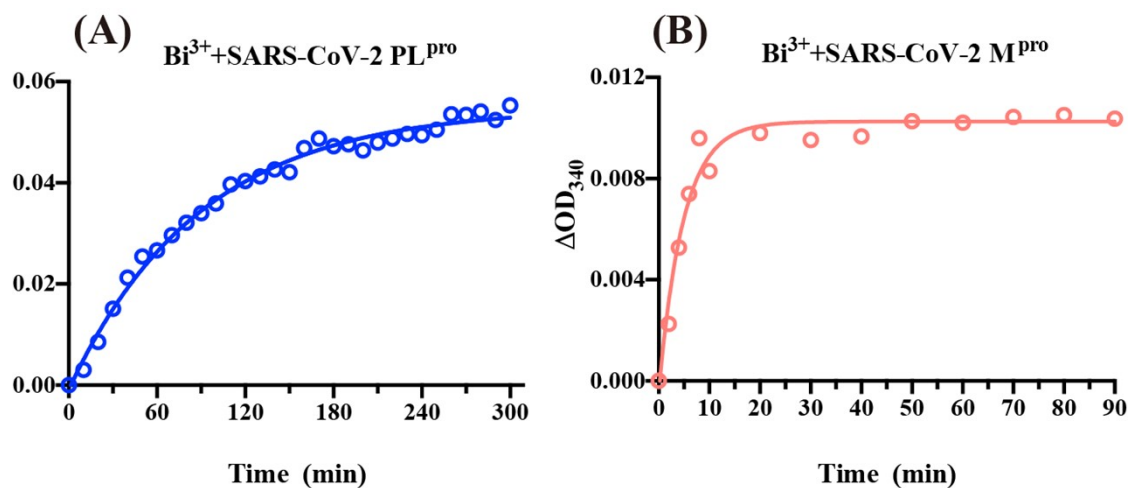


Fig. S9. Binding of Bi^{3+} to SARS-CoV-2 PL^{pro} and SARS-CoV-2 M^{pro}. (a-b) Dependence of absorbance at 340 nm verse time for the reaction of Bi^{3+} (20 mol eq.) with (a) SARS-CoV-2 PL^{pro} and (b) SARS-CoV-2 M^{pro}. CBS was used as the Bi^{3+} source in this assay. The curves were shown as a nonlinear least square fit using a one-phase exponential function by Prism 8.0.

Supplementary Table:**Table S1** Antiviral activity of CBS+3NAC

CoV/cell line	CBS+3NAC*
	EC ₅₀ (± SD) (μM)
SARS-CoV-2/Vero E6	5.83(±0.57)
SARS-CoV-2 (B.1.1.7)/Vero E6	7.43(±1.20)
MERS-CoV/Vero E6	11.26(±2.34)
HCoV-229E/HELFI	21.48(±5.61)

*The measurement of CBS+3NAC content was based on Bi content.

Table S2 Pharmacokinetic parameters of CBS and CBS+10NAC after oral administrations (n= 5).

Pharmacokinetics parameters	CBS*#	CBS+10NAC*#
T_{\max} (\pm SD) (h)	2.53(\pm 2.01)	4.00(\pm 2.74)
C_{\max} (\pm SD) (μ g/L)	447.06(\pm 132.39)	758.81(\pm 251.74)
$AUC_{0 \rightarrow 12 \text{ h}}$ (\pm SD) (h \cdot μ g/L)	1316.94(\pm 474.00)	2750.00(\pm 1151.99)
$AUC_{0 \rightarrow 24 \text{ h}}$ (\pm SD) (h \cdot μ g/L)	2324.20(\pm 759.76)	3616.20(\pm 1553.57)

*Drug dosage used in this study: CBS (150 mg/kg), NAC (610 mg/kg)

#The measurement of CBS and CBS+10NAC was based on Bi content.

Table S3 Enzyme inhibitory activity of CBS+3NAC against SARS-CoV-2

Compound	Inhibitory activity/ IC ₅₀ (± SD) (μM) *				
	ACE2	PL ^{pro}	M ^{pro}	Hel dsDNA-unwinding	Hel ATPase
CBS+3NAC	105.89(±14.39)	1.00(±0.24)	20.10(±1.49)	1.88(±0.29)	1.31(±0.18)
CBS	>5000	1.02(±0.25)	22.25(±2.23)	1.24(±0.02)	1.88(±0.12)
NAC	173.30(±19.31)	>150	>450	>150	>150

*The measurement of CBS and CBS+3NAC was based on Bi content.